

Catalytic partial oxidation of methane over a 4% Rh/ α -Al₂O₃ catalyst Part I: Kinetic study in annular reactor

Alessandro Donazzi, Alessandra Beretta*, Gianpiero Groppi, Pio Forzatti

Laboratorio di Catalisi e Processi Catalitici, Dipartimento di Energia, Politecnico di Milano, Piazza Leonardo da Vinci 32, 20133 Milano, Italy

Received 29 January 2008; revised 13 February 2008; accepted 14 February 2008

Available online 17 March 2008

Abstract

The catalytic partial oxidation (CPO) of CH₄ to synthesis gas over a 4 wt% Rh/ α -Al₂O₃ catalyst was investigated by means of a short contact time annular reactor, specifically designed for testing very fast and exothermic reactions. Data were collected by feeding CH₄/O₂/inert gas mixtures, at varying temperature (from 350 to 850 °C), GHSV (up to 4.5×10^6 Nl/K g_{cat}/h), O₂/CH₄ ratio (from 0.56 to 1.3), reactant dilution (1 to 27% CH₄ v/v) and adding CO₂ (1%) and H₂O (1 and 2%) to the standard feed. Steam reforming, CO₂ reforming, water gas shift (WGS), reverse-WGS, H₂ and CO combustion tests were also carried out to refine the study. A quantitative analysis of the experimental data was performed by a 1D mathematical model of the reactor, wherein a molecular kinetic scheme of the process was incorporated. The scheme consists of CH₄ total oxidation and reforming, the water gas shift and reverse water gas shift reactions, and H₂ and CO post-combustion reactions. On the basis of experimental data and numerical analysis, it was found that, under the CPO conditions: (1) the kinetic role of CO₂ reforming is negligible, so that steam reforming and CH₄ total combustion alone can account for the consumption of CH₄; (2) oxidation and steam reforming of methane have comparable intrinsic kinetics under differential conditions, but surface coverages differently influence the reaction rates under integral conditions; (3) the direct and the reverse water gas shift reactions (WGS and RWGS), when far from the chemical equilibrium, have independent kinetics; (4) the process kinetics is significantly affected by the dilution of the reacting mixture: since the global reaction order is lower than 1, conversion and selectivity decrease at decreasing dilution. Part I of the work deals with the development and the validation of the proposed kinetic scheme; Part II deals with the analysis of CO₂ reforming and RWGS experiments and supports the assumption that CO₂ reforming can be excluded from the CPO kinetic scheme.

© 2008 Elsevier Inc. All rights reserved.

Keywords: CH₄ catalytic partial oxidation; Steam reforming; CO₂ reforming; Rh/ α -Al₂O₃; Synthesis gas; Annular reactor; Kinetic study; Indirect kinetic scheme

1. Introduction

The catalytic partial oxidation of methane to synthesis gas in short contact time reactors is generally addressed as a potentially attractive method for natural gas conversion. CH₄ conversion close to unity and 90% selectivity to H₂ and CO can be reached by oxidizing CH₄ over Rh or Pt structured catalysts at high reaction temperatures (1100 K), at contact times of 10⁻² to 10⁻⁴ s and with autothermal reactor configurations [1]. Autothermal operating conditions yield significant economic, energetic and environmental benefits [2]. The presence of a catalyst allows the attainment of high yields and large

throughput with small reactor sizes and lower operating temperatures; simplicity and compactness of the reactor reduce its heat capacity and improve its dynamic response. All these features make the catalytic partial oxidation (CPO) process ideal for small to medium scale decentralized production of H₂ and syngas. Though extremely flexible, the process is highly complex. Short contact time reactors work under severe conditions, with very high gas hourly space velocity (GHSV) and temperatures, complex fluid pattern and a strong coupling of heat and mass transfer with surface and possibly gas phase kinetics [3]. These factors make the understanding of the process kinetics, a pre-requisite for any design application, a challenging task. As a matter of fact, despite general agreement that rhodium is the best performing element for carbon-free methane partial oxidation [4], a debate is still ongoing on the mechanism

* Corresponding author.

E-mail address: alessandra.beretta@polimi.it (A. Beretta).

of methane activation and the sequence of syngas production. Two distinct mechanisms are proposed for explaining the formation of syngas. The indirect pathway postulates that CH_4 is first totally oxidized to CO_2 and H_2O (a strongly exothermic reaction) and then reformed to produce syngas (with endothermic reactions). One major proof of the existence of such an exothermic–endothermic sequence has been the observation of sharp hot-spot temperatures at the entrance of the reactor [5]. The direct pathway postulates the formation of H_2 and CO as primary products. The main evidence in favor of a direct path is the observation of syngas at extremely short contact times, in the presence of unreacted O_2 [6]. H_2O and CO_2 are in this case interpreted as non-selective oxidation products. The mechanism was proposed to consist of the dissociative adsorption of CH_4 with formation of carbon species and H adatoms, followed by the associative desorption of two H adatoms to H_2 and the oxidation of C to CO [7]. In the literature, depending on the sampling technique, on the type of reactor and on the operating conditions, different product distributions were obtained and different mechanisms were thus inferred, either direct [8–10], indirect [11–13], or mixed [14]. Many factors were speculated to govern the reaction pathway, namely pressure, temperature, change in Rh oxidation state [10,15–18] and nature of the support [10,13,16,19].

Some authors [9,13] used TAP techniques with isothermal conditions, either under vacuum or diluted atmosphere, to maintain a well-defined state of the surface. A common agreement was found on the scarce reactivity of Rh_2O_3 species in the decomposition of CH_4 ; O_2 on the catalyst surface would play a substantial role in determining the direct or indirect pathway. In any case, TAP results are usually obtained under very limited conditions and their extrapolation to higher pressures and concentrations is not straightforward.

Other authors [14,20–22] studied the process under relevant practical conditions, using either autothermal or nonadiabatic reactors and different geometries of the catalyst support (spheres, honeycombs or metal foams). Typically, in these studies the reaction mechanism is inferred from the outlet concentrations. Such an approach is claimed to be not fully rigorous for the mechanism analysis, since frequently both a direct and an indirect scheme can equally justify the data. Recently, a new capillary sampling technique combined with quadrupole mass spectrometry has been developed and applied in autothermal reactors over Rh and Pt foams [23–25]. Spatial and temporal resolved data (0.3 mm and 0.05 s) have been collected inside the catalyst bed under both transient and steady-state conditions. The results have shown that the reactor is divided into a short, initial oxidation zone, where H_2 and CO are produced by direct oxidation in the presence of gas phase O_2 , and a reforming zone, where H_2O reforming is active, CO_2 reforming is absent and the contribution of WGS varies with the C to O feed ratio. Along with the same concept, other techniques have been developed in order to get in situ surface diagnostics during the CPO reaction, using either laser based spectroscopy (Raman and LIF) [26] or X-ray absorption spectroscopy [27,28]. What emerges is that, when adopting more complex and technically

relevant reactors, an effort is needed to isolate heat and mass transport phenomena from the reaction kinetics.

By the means of detailed kinetic modeling, Schwiedernoch et al. [14] suggested that a competition between total oxidation, direct oxidation and steam reforming takes place on the catalysts and that syngas selectivity is highly dependent on oxygen coverage on the surface. Mhadeshwar and Vlachos [29], remarking the importance of thermodynamic consistency in the rate parameters and of a detailed description of adsorbate–adsorbate interactions on the activation energies of surface kinetics, developed a C_1 microkinetic model using a hierarchical multiscale approach. The authors speculated that an oxidation zone exists on the catalyst, followed by a reforming zone. In the oxidation zone, a combination of partial and complete oxidation is active and CO and H_2O are the primary products. H_2 is formed by steam reforming in the reforming zone.

In a previous work [12], the authors addressed a kinetic study of CH_4 -CPO over Rh catalysts at low Rh load, using a novel isothermal annual reactor (specifically designed to study fast and exothermic reactions [30]), wherein heat and mass transfer artifacts are minimized and high space velocities allow to skip the thermodynamic control. The flexibility of this experimental tool was proven by testing CH_4 -CPO in a wide operating field. Strong pieces of evidence were obtained in favor of an indirect kinetic scheme, including the shape of the temperature profiles and the dependence of syngas selectivity on the operating parameters. Data could be well described by a kinetic scheme consisting of methane oxidation, reforming reactions, the reversible WGS reaction, and the consecutive oxidations of H_2 and CO . This simplified kinetic treatment was incorporated in the model of an adiabatic fixed-bed reactor and validated by simulation of a lab-scale autothermal reactor, operating with methane/air mixtures [31].

The aim of the present work is to extend our previous investigations toward the study of highly active Rh catalysts, collect data under well-defined temperature and flow conditions and to enlarge the basis for the kinetic analysis of the CPO process. A kinetic study of the catalytic partial oxidation of CH_4 over a 4 wt% Rh/ α - Al_2O_3 catalyst was performed in a short contact time annular reactor. This reactor configuration allowed operating far from thermodynamic constraints, with good control of mass transfer and with a simple flow pattern. Most importantly, the catalyst superficial temperature was measured and temperature profiles were collected along the axis of the layer with a 2 mm resolution. Data were obtained at high space velocity in a wide range of temperatures (300–850 °C) and compositions, focusing on those aspects that the previous investigation had not fully addressed (e.g., the role of WGS and its reverse reaction, the relative importance of steam and dry reforming, the overall kinetic order of the process). A comprehensive experimental design was carried out with diluted mixtures under nearly isothermal conditions; it consisted of tests of CPO, steam reforming, CO_2 reforming, WGS, reverse-WGS, H_2 and CO oxidation. Additionally, CPO tests at decreasing dilution were carried out in order to bridge the gap between kinetics of diluted feed streams and kinetics of concentrated CH_4 /air streams. The purpose was the development of a reliable molecular kinetic

scheme, with minimum correlation among the parameters and sufficient robustness for design applications. The whole work is reported in a two-paper series. The first paper illustrates the CPO and the side reactions experiments, as well as the development of a molecular kinetic scheme. The second paper focuses on the relative rate of steam and dry reforming; based on the comparative analysis of steam reforming, CO₂ reforming and RWGS tests, the paper supports the assumption that CO₂ reforming can be neglected in the kinetic scheme of CH₄-CPO.

2. Experimental

2.1. Catalyst preparation

α -Al₂O₃ was used as thermally stable support. It was prepared by calcining a commercial γ -Al₂O₃ (Puralox Sba-200, Sasol) in air at 1100 °C for 10 h. Phase composition was verified by XRD, superficial area (9 m²/g) by BET analysis (Tristar Micromeritics) and pore size distribution by Hg porosimetry (Micromeritics AuotoPore IV). The pore size distribution was centered on a pore diameter of 100 nm; the pore volume amounted to 0.4 cm³/g. A 4% Rh/ α -Al₂O₃ sample was prepared by dry impregnation of the α -Al₂O₃ support with a commercial Rh(NO₃)₃ solution (14.68 wt% Rh, Chempur); the impregnated support material was dried at 110 °C for 3 h. The catalytic powders were deposited in the form of thin layers (15–30 μ m) on alumina tubular supports by a dip-coating standard procedure, described in detail elsewhere [32], which can be briefly summarized as follows: a slurry was prepared by adding the catalyst powders to an acidic solution (HNO₃/powder = 1.7 mmol/g, H₂O/powder = 1.7 g/g) and was ball-milled for 24 h; the alumina tubular support was coated on its terminal portion (2 cm from the sealed end) by dipping into the slurry and extraction at constant velocity; the coated tube was dried at 280 °C for 10 min (flash-drying) obtaining a well adhered catalyst layer. Rh loading of the catalyst was verified by atomic adsorption analysis of the flash-dried powders.

2.2. Testing apparatus

The kinetic tests were performed in an annular duct reactor [30] which was externally heated by a three zone Carbolite oven. The reactor (Fig. 1) was assembled as follows: the catalyst-coated alumina (O.D. 4 mm) was coaxially inserted into a quartz tube (I.D. 5 mm) giving rise to an annular duct (0.5 mm channel height) through which the gas flowed in laminar regime. The reactor design allowed operating at very high GHSV (10^6 – 10^7 Nl/K g_{cat}/h) with negligible pressure drops. Temperature profiles were measured by sliding a thermocouple (K-type) inside the alumina tube itself. Thermal equilibrium across the alumina tube section ensured the correspondence between the measured temperature and the catalyst temperature, due to the negligible contribution of the thermal dispersion along the alumina tube on the overall heat dissipation [33]. The catalyst average temperature was calculated as an arithmetic average of the single measurements taken every 2 mm along the length of the layer (2 cm). In all the figures, data are reported as a function of the catalyst average temperature unless otherwise specified. Oven temperatures were recorded by a second K-type thermocouple sliding in a mullite tube which was placed along the heating wall. At high temperature, an efficient mechanism of reaction heat dissipation by radiation allowed keeping the temperature gradients below 10 °C/2 cm when dealing with diluted feed mixtures, so that nearly isothermal conditions could be assumed during the kinetic tests. In the case of non-diluted feed streams, thermal gradients could not be neglected and the axial temperature profiles (measured with 2 mm spatial resolution) were accounted for during the kinetic analysis. Gas flow into the reactor was controlled by mass flow controllers (BROOKS mass flow meters) and heated (120 °C) stainless steel lines were used to carry the gas mixture. A micro-GC (3000 A, Agilent Technologies) was used to analyze the inlet and the outlet gas compositions; it was equipped with two isothermal capillary columns and two thermal conductivity detectors (TCD). N₂, H₂, O₂, CH₄ and CO were separated by a Molecular Sieve 5 Å column (180 °C) with Ar as a car-

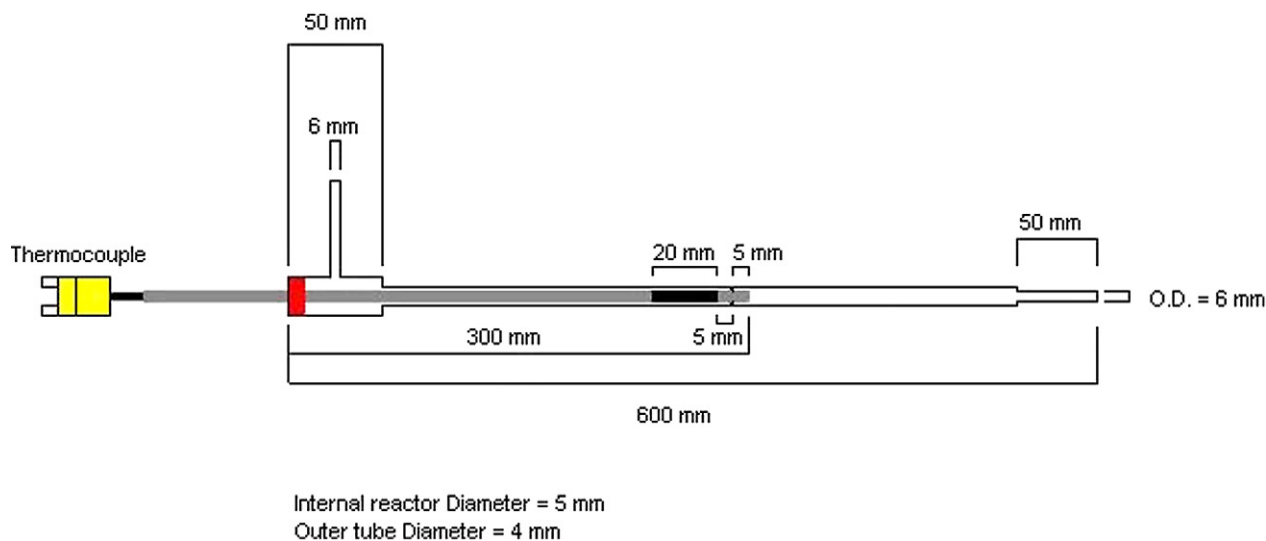
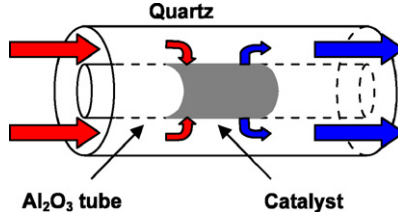


Fig. 1. Sketch of the annular reactor.

Table 1
Model equations

	Mass balance equation, bulk phase (<i>i</i> th species):
	$Pe_{m,i} \frac{dF_i^*}{dz^*} = - \frac{4}{1 + \frac{1}{R^*}} Sh_{10c_i} (x_i^B - x_i^W) \frac{F_{TOT}^*}{F_{TOT}^0} \quad (1)$
	Continuity equation, catalyst phase (<i>i</i> th species):
	$Sh_{10c_i} (x_i^B - x_i^W) = \sum_{j=1}^{NR} v_{i,j} \alpha_i R_j \quad (2)$
	Mass transfer coefficient:
	$Sh_{10c,i} = Sh_{inf} + 6.874 \exp(-71.2z_{Sh,i})(1000z_{Sh,i})^{-0.35} \quad (3)$

Generalized internal efficiency:

$$\eta_{O_2}^\infty = \frac{\sqrt{2}}{\delta_L r_{O_2} (C_{O_2}^S)} \sqrt{\int_0^{C_{O_2}^S} D_{eff,O_2} r_{O_2}(C) dC}, \quad \phi_{O_2} = \frac{1}{\eta_{O_2}^\infty}, \quad \eta_{O_2} = \frac{\tanh(\phi_{O_2})}{\phi_{O_2}} \quad (4)$$

$$\eta_{CH_4}^\infty = \frac{\sqrt{2}}{\delta_L r_{CH_4} (C_{CH_4}^S)} \sqrt{\int_{C_{CH_4}^{S,eq}}^{C_{CH_4}^S} D_{eff,CH_4} r_{CH_4}(C) dC}, \quad \phi_{CH_4} = \frac{1}{\eta_{CH_4}^\infty}, \quad \eta_{CH_4} = \frac{\tanh(\phi_{CH_4})}{\phi_{CH_4}} \quad (5)$$

Effective diffusivity coefficient:

$$D_{eff,i} = \varepsilon_M^2 D_{M,i} + \frac{\varepsilon_\mu^2 (1 + 3\varepsilon_M)}{1 - \varepsilon_M} D_{\mu,i} \quad (6)$$

Axial temperature profile:

$$T(z) = a_1 z^5 + a_2 z^4 + a_3 z^3 + a_4 z^2 + a_5 z + a_6 \quad (7)$$

Note. Index *i* = CH₄, O₂, CO, CO₂, H₂, H₂O. Equation (7) is included for simulation of non-isothermal experiments only; coefficients *a*₁–*a*₆ are estimated by fitting the polynomial expression to the measured temperature profile of the single experiment.

rier, while CO₂ and H₂O were separated by a Plot Q column (160 °C) fed with He. C₂H₆, C₂H₄ and C₂H₂ were never detected during the tests. For quantitative determination of the concentrations, N₂ was used as an internal standard. Blank experiments on a bare alumina tube verified the chemical inertness of the ceramic support and the absence of gas phase reactions below 850 °C. In all the runs, the product gas C, H and O balances closed to within ±5%.

2.3. Operating conditions

All the experiments were performed at atmospheric pressure. A typical run consisted of varying the oven temperature from 300 up to 850 °C, with step-wise increments of 10–50 °C. At each temperature, conversions and selectivities were measured by repeated analyses and showed stable values within 15–20 min: prior to the kinetic investigation, the catalyst underwent a standard conditioning procedure which consisted of repeated runs at GHSV of 8×10^5 Nl/K g_{cat}/h, feeding a di-

luted gas mixture with composition CH₄ = 4% v/v, O₂/CH₄ = 0.56, N₂ to balance; the catalyst conditioning was complete when stable performances were reached in the whole temperature range. To contrast the thermodynamic control, experiments were performed at higher values of GHSV than the conditioning one; since the increase of GHSV makes axial thermal gradients more pronounced, further dilution of the reacting mixture was necessary in order to realize quasi-isothermal conditions. Standard reaction conditions consisted of 1% CH₄ v/v, O₂/CH₄ = 0.56, N₂ to balance and a GHSV of 2×10^6 Nl/K g_{cat}/h.

2.4. 1D mathematical model of the annular reactor

Experimental results were analyzed by a one-dimensional, heterogeneous model of the reactor, whose governing equations, boundary conditions and transport correlations are reported in dimensionless form in Table 1. Plug flow mass balances were used for the gas phase (Eq. (1)), while the solid phase was described through steady-state equations of conti-

nity between the catalyst wall and bulk (Eq. (2)), in which the radial mass flow of each species was equated to its overall formation rate. Due to the high axial Péclet number, axial diffusion was neglected in the gas phase. Inter-phase and intra-phase mass transfer limitations were both accounted for, so that it was possible to decouple the reaction kinetics from the contributions of mass transfer. Inter-phase resistances were described through a functional form for the local Sherwood number (Eq. (3)) which was used in the literature to interpolate the exact solutions of Greatz–Nusselt problems and equivalent mass transfer problems in annular ducts with third type boundary conditions [34]. Intra-phase mass resistances were described using generalized efficiency factors (Eqs. (4)–(5)) for O₂ and CH₄; η_{O_2} was calculated on the basis of the overall oxygen consumption rate, while η_{CH_4} on the basis of the reforming rate. The oxidation rates were assumed to be limited by O₂ while the reforming rate by CH₄ and these effects were included by multiplying each rate for the correct η_i factor. Molecular diffusivities were approximated as binary diffusivities of each i species in N₂, according to the Fuller–Schettler–Giddings correlation [35]. O₂ and CH₄ effective diffusivities were evaluated according to the Wakao–Smith random pore model (Eq. (6)), assuming an average macro-pore radius of 200 nm with a macro-void fraction of 5% and an average micro-pore radius of 50 nm with a micro-void fraction of 0.55; a bimodal distribution was assumed for the pores, in which the macro-porosity term described the inter-granular α -Al₂O₃ distance and the micro-porosity term accounted for the α -Al₂O₃ porosity, measured by Hg intrusion. When the overall temperature difference along the catalyst bed was below 10 °C, the isothermal approximation was satisfactory and the catalyst temperature was taken as the average. For non-isothermal experiments, the actual temperature profile on the layer was accounted for with a fifth-order polynomial function in the axial coordinate, which best interpolated the data (Eq. (7) in Table 1).

3. Experimental results

3.1. CPO test with highly diluted feed

3.1.1. Effects of temperature and GHSV

CH₄ partial oxidation tests were performed with diluted feed streams (CH₄ = 1%, O₂/CH₄ = 0.56, N₂ to balance) in the temperature range 300–850 °C at varying gas space velocity from 8×10^5 to 4.5×10^6 Nl/K g_{cat}/h. Results are reported in symbols in Fig. 2, wherein the molar fractions of reactants and products are plotted against the catalyst average temperature. The reaction started at 300 °C; with increasing temperature, the conversion of CH₄ and O₂ grew. At temperatures below 400–500 °C (depending on the flow rate value), CO₂ and H₂O were the only detectable products. As O₂ conversion was complete, a decrease of the CO₂ and H₂O molar fractions was observed, syngas production began and increased steadily with increasing temperature and increasing CH₄ consumption, until reaching of the equilibrium composition. At increasing GHSV, the conversion of CH₄ and O₂ decreased and the temperature for complete O₂ conversion grew. The decrease of conversion

was accompanied by a decrease of H₂ and CO selectivities. As observed in analogous experiments of CH₄ CPO on a 0.5% Rh/Al₂O₃ catalyst [12], the measured axial temperature profiles (Fig. 3) were characterized by the presence of a hot spot upon increasing the average temperature, up to complete O₂ conversion; on further increasing the catalyst temperature, the hot spot moderated, moved back toward the inlet of the layer and was followed by a progressive decrease of the temperature. Nevertheless, the maximum axial gradient of the layer was kept within 5 °C/cm and the experiments could be considered nearly isothermal.

3.1.2. Effect of H₂O co-feed

H₂O-enriched CPO tests were performed by actually co-feeding a stoichiometric amount of H₂ and O₂ to the standard CPO mixture. As shown in Fig. 4, H₂ oxidation was already complete at 300 °C and at the higher investigated temperatures it presumably occurred at the inlet section of the layer. This solution allowed a good control in the feed of small fluxes of H₂O, better than the use of a pump or a saturator. Thus, in order to obtain an *in situ* production of 1% and 2% H₂O, the real feed compositions were respectively CH₄/O₂/H₂ = 1/1.06/1 and CH₄/O₂/H₂ = 1/1.56/2 v/v, N₂ to balance. Fig. 4 reports the observed results. In the presence of 1% H₂O, the activation of CH₄ and O₂ in the low temperature range was delayed; at the same temperatures, the increase of H₂O concentration up to 2% had a minor effect. Above 450 °C, i.e. upon reaching complete O₂ oxidation, the addition of H₂O had no effect on the conversion of CH₄, despite the thermodynamic driving force (indeed, the equilibrium conversion of CH₄ is expected to increase at increasing H₂O content). Upon increasing the H₂O content, larger yields of H₂ and CO₂ were observed with a decrease of CO production, which could be related to the thermodynamic effect of H₂O on the equilibrium of the WGS reaction.

3.1.3. Effect of CO₂ co-feed

CO₂-enriched tests were carried out by adding 1% CO₂ to the standard reacting mixture (1% CH₄, O₂/CH₄ = 0.56, 2×10^6 Nl/K g_{cat}/h); CO₂ was fed directly from a cylinder. In the whole temperature range (350–850 °C) no effect was detected on the conversion of reactants (Fig. 5), while the product distribution changed following the thermodynamics of WGS. CO₂ addition had no consequences on the temperature profiles, which were maintained nearly unchanged. It is worth noting that the catalyst did not suffer from any deactivation after the exposure to the CO₂-rich mixture, as it was verified by repeating a CPO run under standard conditions.

3.1.4. Effect of O₂/CH₄ feed ratio

Tests with 1% and 1.3% O₂ inlet fraction were carried out at 2×10^6 Nl/K g_{cat}/h, while keeping CH₄ concentration at 1% v/v. As shown in Fig. 6, the conversion of CH₄ was not affected by the increase of the O₂/CH₄ ratio in the low temperature range (300–450 °C). Above 450 °C, a minor promoting effect of the O₂/CH₄ ratio on CH₄ conversion was observed. Passing from 0.56 to 1.3% O₂ inlet concentration, O₂ conver-

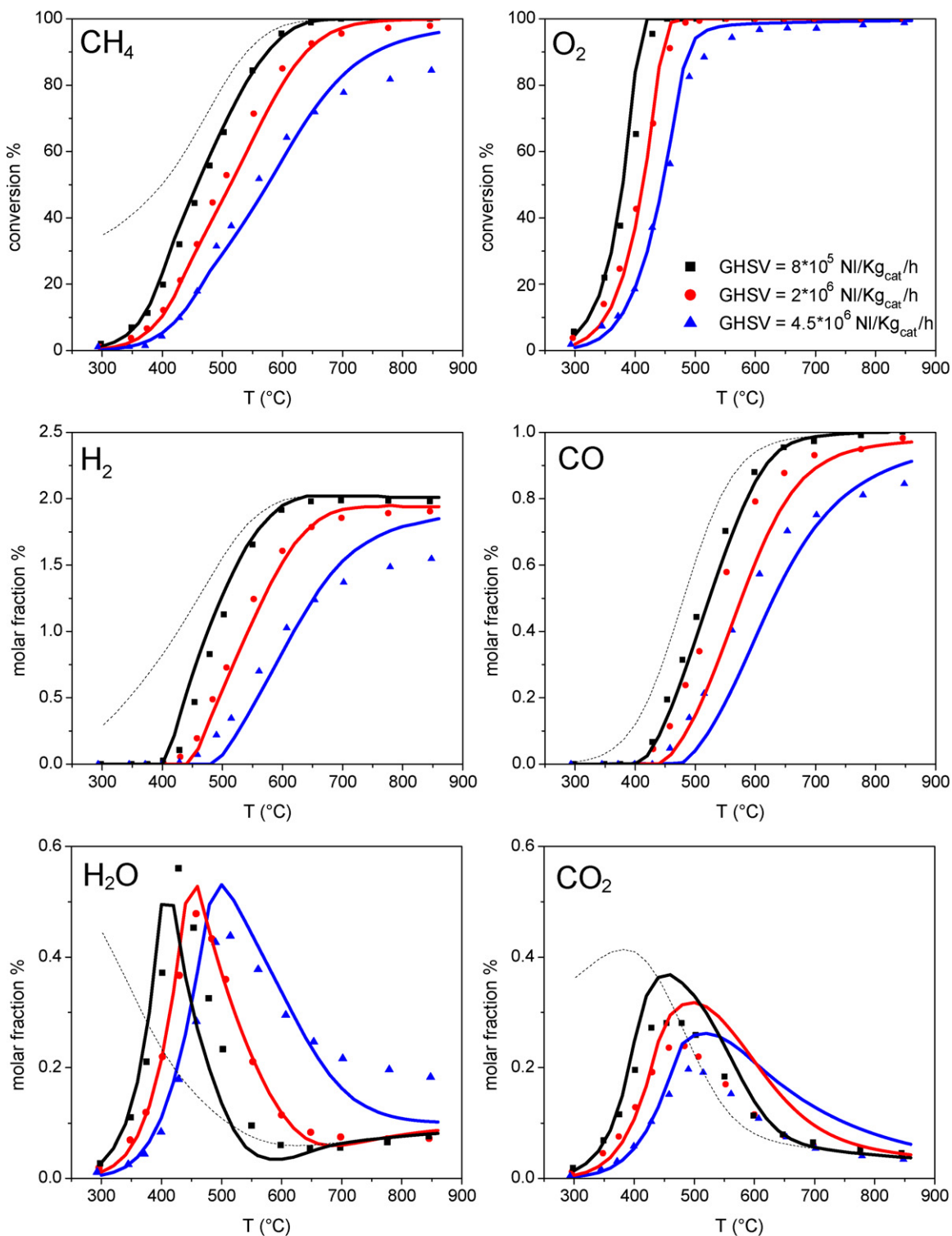


Fig. 2. Effect of GHSV on reactants and products molar fractions. Experimental (symbols) and calculated (solid lines) fractions are reported. (■) GHSV = 8×10^5 Nl/K_{g_{cat}}/h; (●) GHSV = 2×10^6 Nl/K_{g_{cat}}/h; (▲) GHSV = 4.5×10^6 Nl/K_{g_{cat}}/h; (dashed line) equilibrium. Feed composition: CH₄ = 1% v/v, O₂/CH₄ = 0.56, N₂ to balance; atmospheric pressure.

sion decreased and its complete consumption shifted from 480 to 520 °C. Concerning the production of syngas, this began between 400 and 450 °C, while O₂ was still present in the product mixture. A moderate shift to higher temperatures was thus detected upon increasing the O₂/CH₄ feed ratio.

3.2. CPO test at varying dilution

CPO tests were carried out with concentrated CH₄/O₂ mixtures, at 2×10^6 Nl/K_{g_{cat}}/h, varying CH₄ inlet fraction from 1 to 27% and keeping O₂/CH₄ constant at 0.56. Fig. 7 reports re-

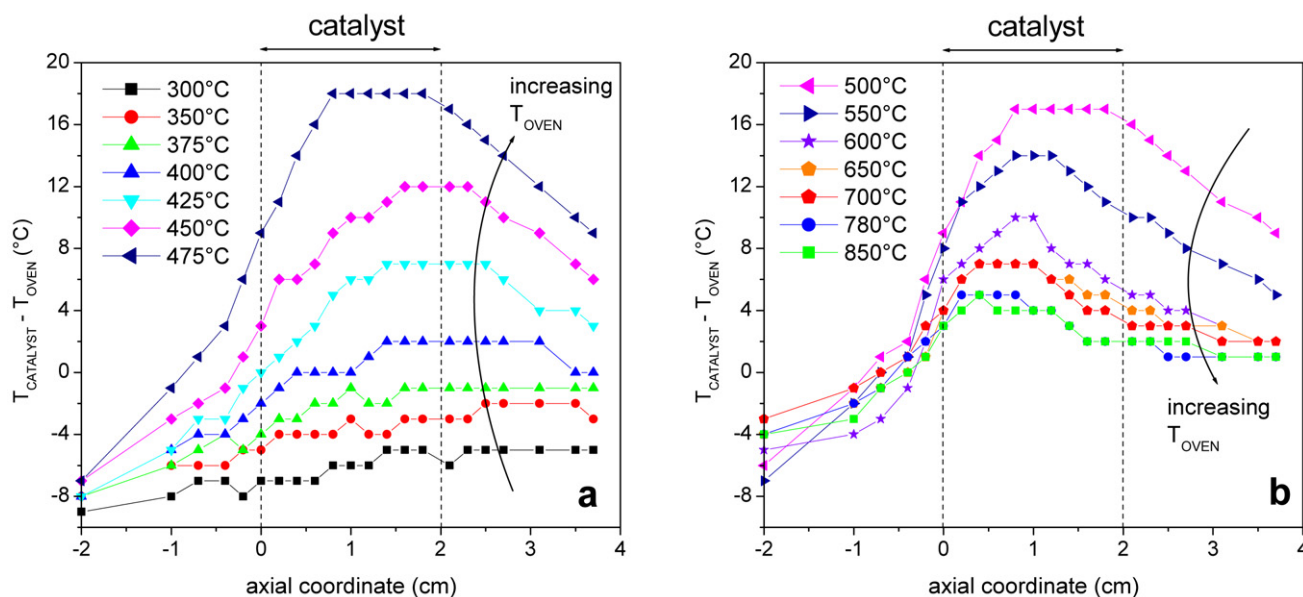


Fig. 3. Temperature profile on the catalyst layer at varying the oven set temperature. Operating conditions: GHSV = 4.5×10^6 Nl/K g_{cat}/h, CH₄ = 1% v/v, O₂/CH₄ = 0.56, N₂ to balance, atmospheric pressure.

actants conversions and product distribution against the average catalyst temperature. The increase of the reactants concentration caused a decrease of both CH₄ and O₂ conversions; the temperature of the complete consumption of O₂ passed from 450 to 580 °C. However, it is worth noting that, within 400 and 550 °C, due to the dramatic boost in the hot spot realized under concentrated conditions (CH₄ > 8.5%), in correspondence of the abrupt rise of O₂ conversion no data could be collected. Upon increasing the reactants concentration, syngas selectivity decreased and higher yields of the total oxidation products were recorded. As well, H₂/CO ratio (Fig. 8a) decreased and reached the equilibrium value at progressively higher temperatures. A similar trend was observed for the WGS K_P/K_{EQ} ratio (Fig. 8b), which, going from 1% to 27% CH₄ inlet fraction, approached unity (the thermodynamic limit) at progressively higher temperatures. At increasing concentration of reactants, the measured axial temperature gradients became more and more significant, with pronounced hot spot temperatures. Fig. 8c reports the evolution of the temperature profile at increasing oven temperature under the most severe conditions, that is the CH₄/air run; at 400 °C oven temperature, the maximum catalyst temperature amounted to 620 °C and the difference between maximum and minimum temperature along the layer hit 132 °C. Fig. 8d shows the maximum ΔT (defined as the difference between the maximum and the minimum measured temperature within the layer) registered at each average catalyst temperature upon increasing the concentration.

3.3. H₂- and CO-rich oxidation tests

The previous study on a low Rh content catalyst [12] pointed out the important kinetic roles of H₂ and CO consecutive oxidations within the CPO process. Accordingly, H₂- and CO-rich oxidation tests were performed on the catalyst herein exam-

ined. H₂-rich oxidation tests were carried out at 20–350 °C, with 2% H₂ v/v and O₂/H₂ ratio of 0.25, at GHSVs of 2×10^6 and 4×10^6 Nl/K g_{cat}/h. Fig. 9a reports H₂ conversion against the catalyst average temperature: H₂ conversion gradually increased until reaching the light off temperature at about 80–100 °C, where an abrupt growth was registered. Afterward, above 110 °C, the slope of the H₂ conversion curve moderated, possibly due to the effect of O₂ mass transfer limitations. H₂ conversion decreased upon increasing the GHSV, while the reaction light off occurred at the same temperature. CO combustion tests were performed at 100–550 °C under rich conditions (CO/O₂/N₂ = 1/0.4/98.6) at GHSVs of 8×10^5 , 2×10^6 and 4×10^6 Nl/K g_{cat}/h. Results are reported in Fig. 9b. Also the curves of CO conversion versus increasing temperature had a sigmoidal shape, still rather narrow, but subject to the onset of O₂ mass transfer at higher temperature (175–225 °C).

3.4. CH₄ + H₂ + O₂: steam reforming tests

Steam reforming tests were carried out by feeding CH₄/H₂/O₂ mixtures with H₂/O₂ in stoichiometric ratio, in order to generate water *in situ* with the proper amount. Three different H₂O/CH₄ ratios were tested (1.5, 2, 2.5) with an inlet CH₄ concentration of 1% v/v and GHSV of 2×10^6 Nl/K g_{cat}/h. Fig. 10 shows that O₂ conversion was complete in the whole temperature range, suggesting that H₂O was produced on a thin catalyst inlet zone before CH₄ reacted. The reaction began at 350–400 °C. CH₄ and H₂O conversions progressively increased with temperature and reached equilibrium at 850 and 700 °C, respectively. The results show a complete overlap of CH₄ conversion curves upon increasing H₂O concentration. CO and H₂ molar fractions monotonically increased with temperature, while CO₂ production passed through a maximum due to the thermodynamics of the WGS reaction. Co-

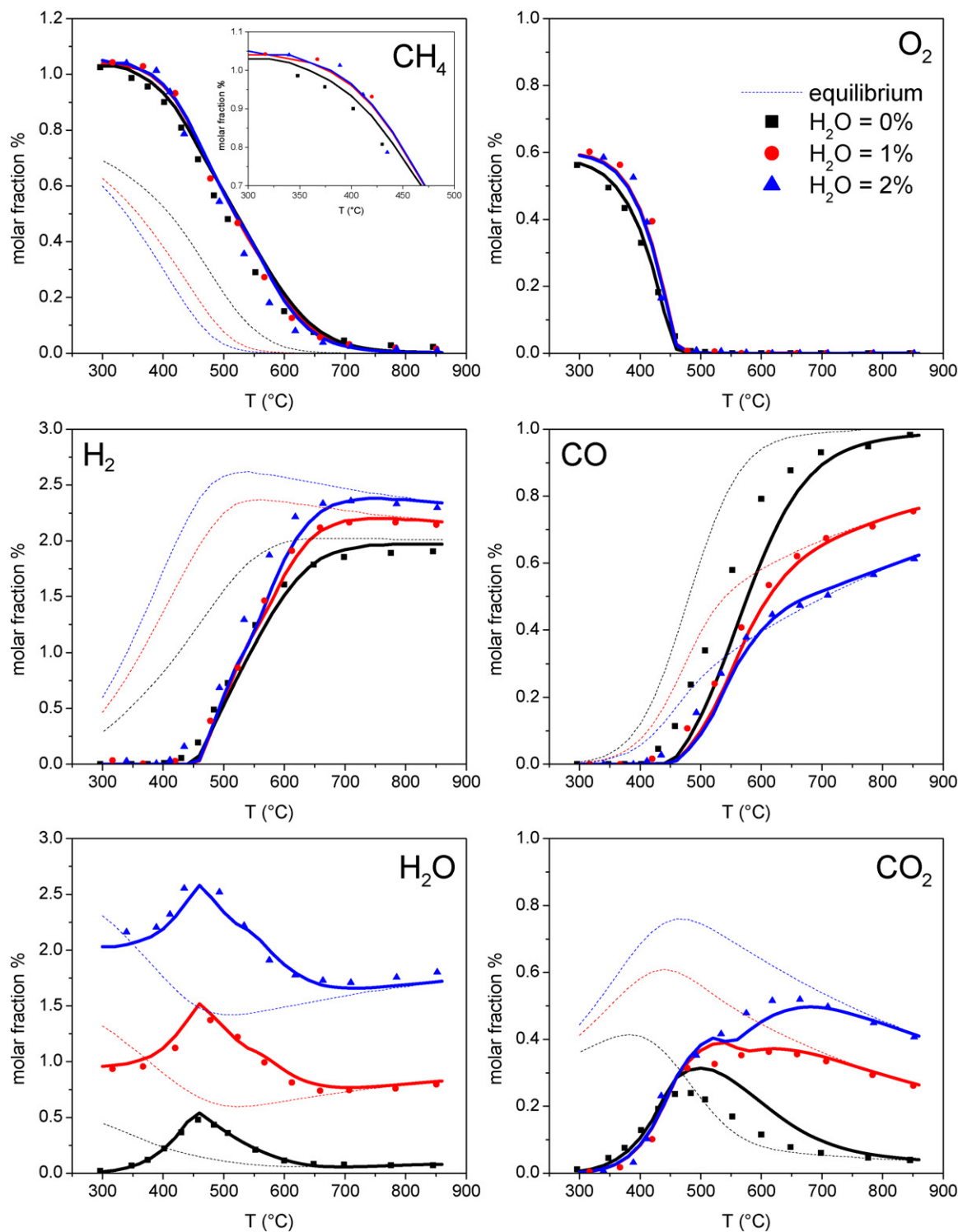


Fig. 4. Effect of H₂O addition on reactants conversions and product molar fractions. Experimental (symbols) and calculated (solid lines) results are reported. (■) 0% H₂O; (●) 1% H₂O; (▲) 2% H₂O; (dashed line) equilibrium. Feed composition: CH₄ = 1% v/v, O₂/CH₄ = 0.56, H₂O variable, N₂ to balance; atmospheric pressure.

herently with the presence of a WGS route, CO₂ syngas production began together with that of syngas. While CO molar fraction decreased with increasing H₂O/CH₄ ratio, H₂ production was scarcely influenced by water addition; the H₂/CO ratio was always larger than 3 and approached the equilibrium above 500 °C.

3.5. WGS tests

WGS experiments were carried out by feeding mixtures with different H₂O and CO inlet fractions at 2×10^6 Nl/K g_{cat}/h: CO/H₂O/N₂ = 4/2.7/93.3, CO/H₂O/N₂ = 1.5/2.3/96.2, CO/H₂O/N₂ = 1.5/3.5/95. H₂O was fed by delivering a flow of

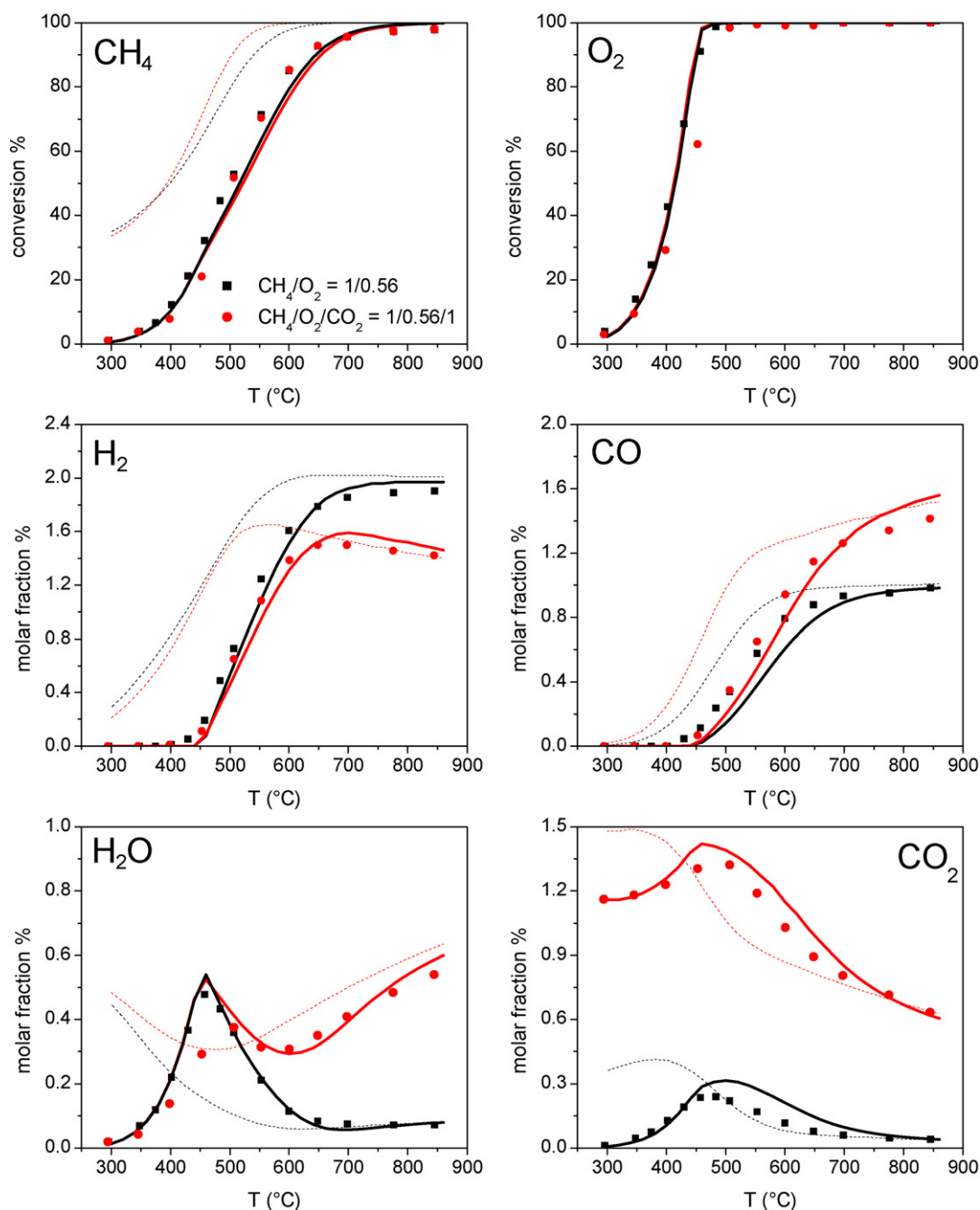


Fig. 5. Effect of CO_2 addition on reactants conversions and product molar fractions. Experimental (symbols) and calculated (solid lines) results are reported. (■) 0% CO_2 ; (●) 1% CO_2 ; (dashed line) equilibrium. Feed composition: $\text{CH}_4 = 1\%$ v/v, $\text{O}_2/\text{CH}_4 = 0.56$, CO_2 variable, N_2 to balance; atmospheric pressure.

N_2 in a saturator before it entered in the reactor. Experiments were performed at temperatures lower than 500°C . Fig. 11 reports in symbols the results. The reaction was under kinetic control in the investigated temperature range, since the measured conversions were much lower than the equilibrium values. H_2O conversion slightly changed upon increasing either the CO content from 1.5 to 4%, or the H_2O content from 2.3 to 3.5%; instead, the conversion of CO decreased at increasing CO concentration and kept almost constant at varying H_2O concentration.

4. Discussion

Most of the observed trends are consistent with an indirect reaction scheme. For CPO, in the presence of residual O_2 , H_2O and CO_2 were the only products; the evolution of their outlet mole fractions at varying temperature, total flow rate and dilution was typically that of intermediate species, while the production of CO and H_2 was clearly consecutive. Only at O_2/CH_4 ratios exceeding 0.56, syngas was formed at $450\text{--}500^\circ\text{C}$ under non-complete conversion of O_2 . At those temperatures, however, the impact of mass transfer limitations is important, re-

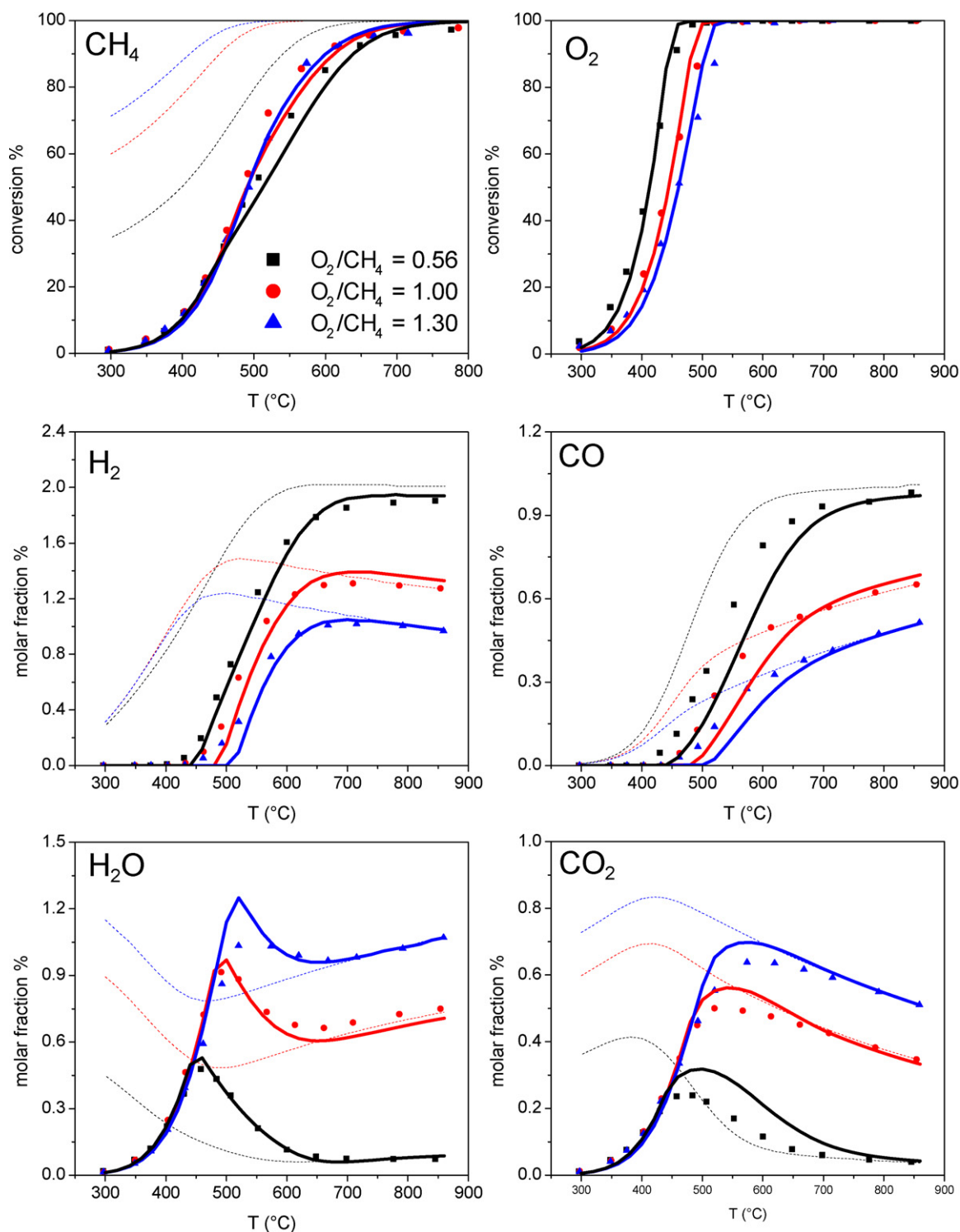


Fig. 6. Effect of O_2/CH_4 molar ratio on reactants conversions and product molar fractions. Experimental (symbols) and calculated (solid lines) results are reported. (■) $O_2/CH_4 = 0.56$; (●) $O_2/CH_4 = 1$; (▲) $O_2/CH_4 = 1.3$; (dashed line) equilibrium. Feed composition: $CH_4 = 1\%$ v/v, O_2/CH_4 variable, N_2 to balance; atmospheric pressure.

sulting in values of O_2 concentration close to zero at the catalyst wall.

In all the CPO experiments, the shape of the measured temperature profiles was also informative. A hot spot grew upon increasing the catalyst average temperature up to the complete consumption of O_2 . On further increasing the catalyst temper-

ature, the hot spot moderated, moved backward to the inlet of the layer and was followed by a progressive decrease of the temperature. These trends suggest the occurrence of a sequence of exothermic and endothermic reactions.

These results agree with those collected in previous works over $Rh/\alpha-Al_2O_3$ catalysts with lower Rh load [12,32]. Never-

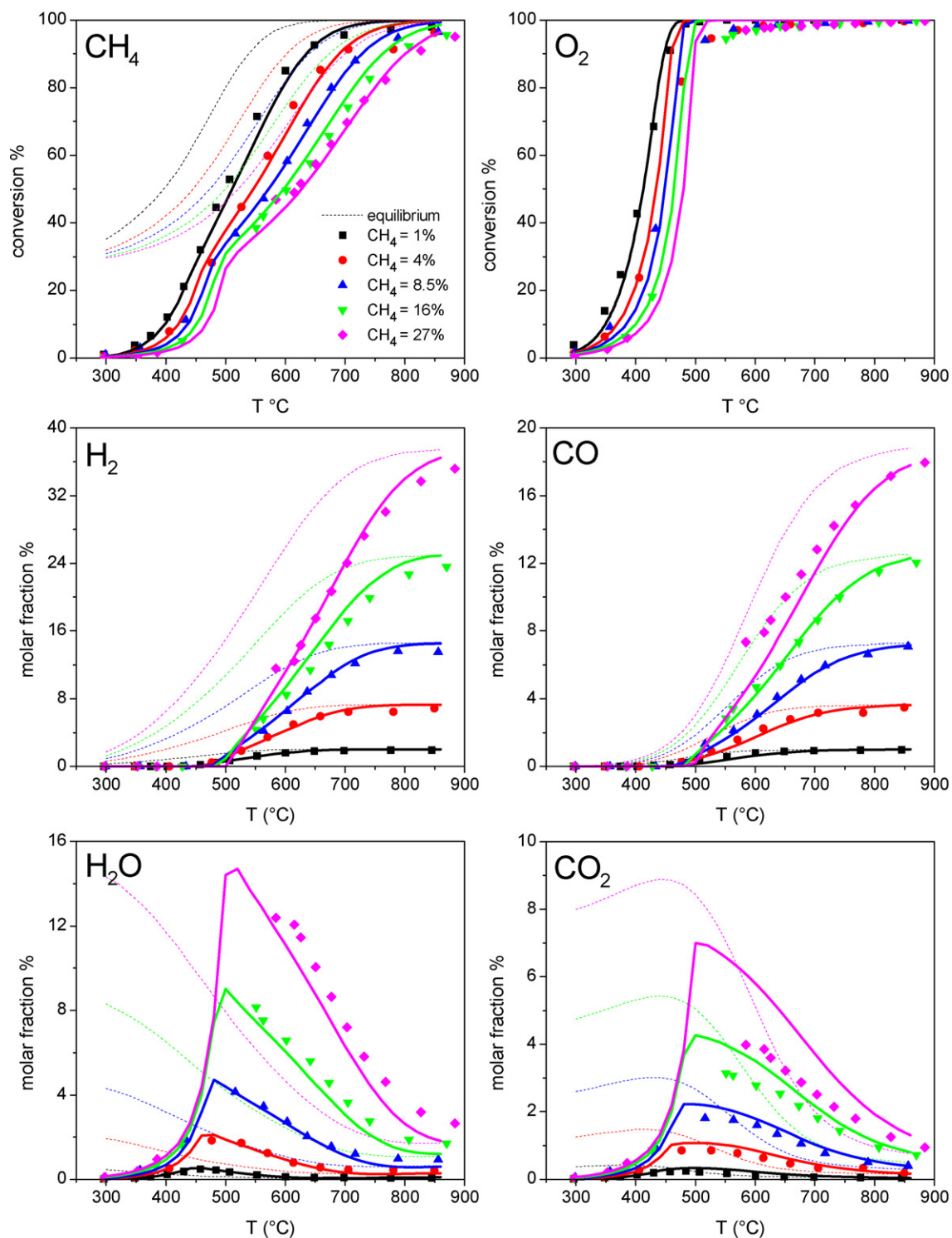


Fig. 7. Effect of dilution on reactant conversion in CPO tests. Experimental (symbols) and calculated (solid lines) fractions are reported. Feed composition: (■) $\text{CH}_4 = 1\%$; (●) $\text{CH}_4 = 4\%$; (▲) $\text{CH}_4 = 8.5\%$; (▼) $\text{CH}_4 = 16\%$; (◆) $\text{CH}_4 = 27\%$ v/v; $\text{CH}_4/\text{O}_2 = 0.56$, N_2 to balance, $\text{GHSV} = 2 \times 10^6 \text{ N l/K g}_{\text{cat}}/\text{h}$, atmospheric pressure.

theless, in the present work the extremely wide range of conditions adds new pieces of evidence which improves the understanding of the process kinetics and shows some unique features of high Rh loading catalysts. The proposed molecular kinetic scheme, the rate equations and their parameters are listed in Table 2. Initial estimates of the rate constants were obtained by

adapting the single kinetic expressions of each reaction to the corresponding experimental pool; thus, the parameters involved in the total oxidation of methane, k_{OX} and $K_{\text{H}_2\text{O}}$, were first estimated on the basis of the low-temperature CPO tests, k_{SR} and K_{CO} from the steam reforming experiments, k_{WGS} from the steam reforming and the water gas shift experiments, k_{RWGS}

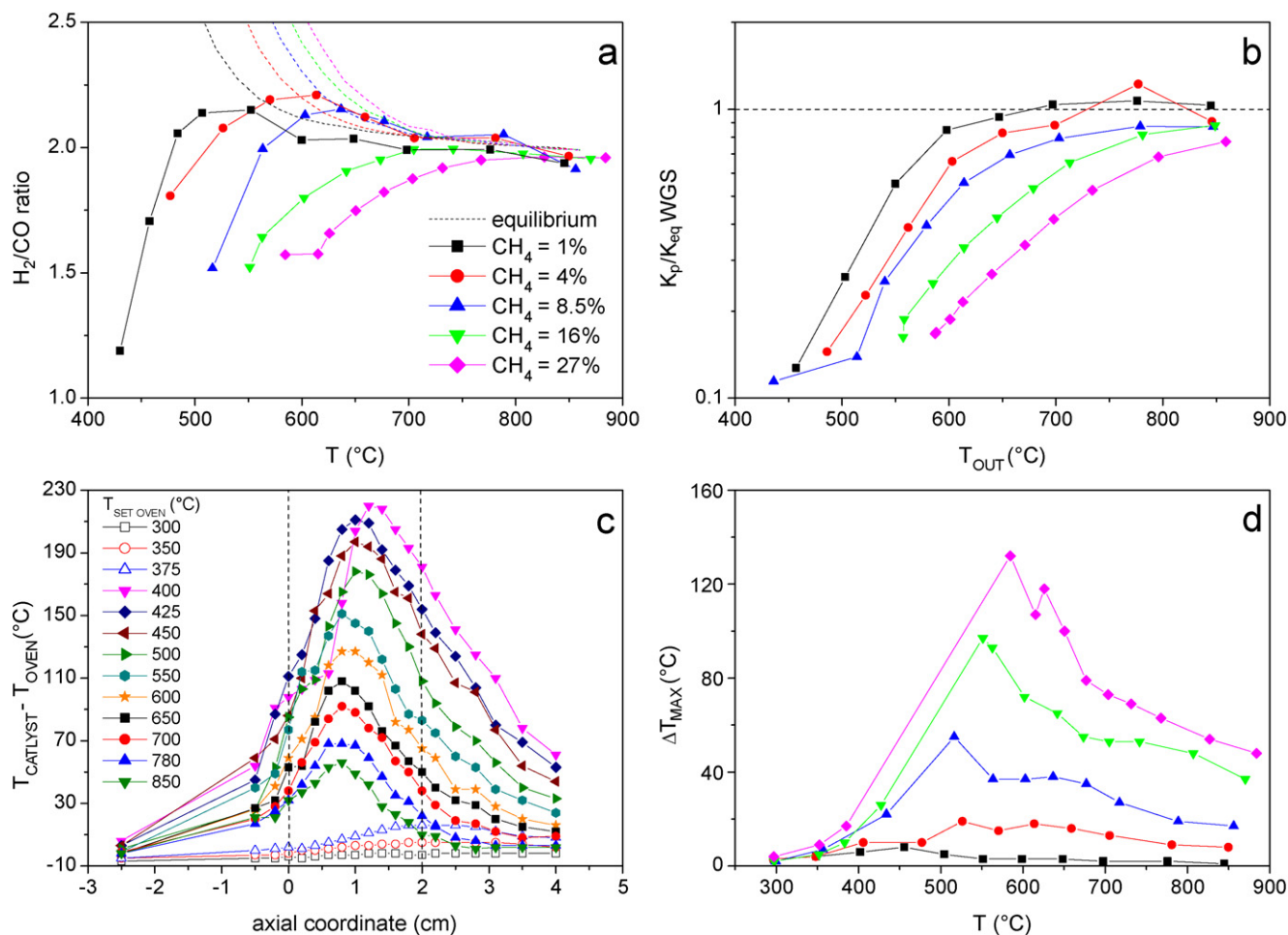


Fig. 8. (a) Effect of dilution on the H_2/CO ratio in CPO tests. (b) Effect of dilution on the WGS K_p/K_{EQ} ratio. (c) Temperature profile on the catalyst layer at varying the oven set temperature at $CH_4 = 27\%$. (d) Maximum axial gradients on the catalyst layer as a function of the average catalyst temperature at different dilution of the reactants. Feed composition: (■) $CH_4 = 1\%$; (●) $CH_4 = 4\%$; (▲) $CH_4 = 8.5\%$; (▼) $CH_4 = 16\%$; (◆) $CH_4 = 27\%$ v/v; $CH_4/O_2 = 0.56$, N_2 to balance, $GHSV = 2 \times 10^6$ $Nl/Kg_{cat}/h$, atmospheric pressure. Effects of $GHSV$ and dilution on the H_2/CO ratio in CPO tests.

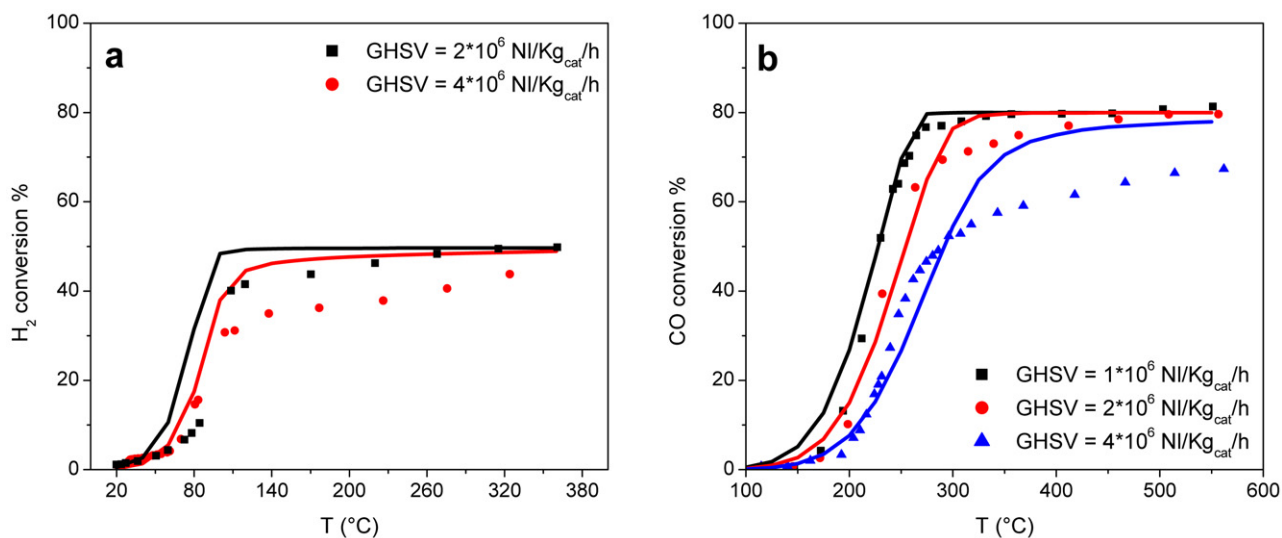


Fig. 9. (a) H_2 conversion in H_2 oxidation tests at different $GHSV$. (■) $GHSV = 2 \times 10^6$ $Nl/Kg_{cat}/h$; (●) $GHSV = 4 \times 10^6$ $Nl/Kg_{cat}/h$. Feed composition: $H_2 = 2\%$ v/v, $O_2/H_2 = 0.25$, N_2 to balance; atmospheric pressure. (b) CO conversion in CO oxidation tests at different $GHSV$. (■) $GHSV = 1 \times 10^6$ $Nl/Kg_{cat}/h$; (●) $GHSV = 2 \times 10^6$ $Nl/Kg_{cat}/h$; (▲) $GHSV = 4 \times 10^6$ $Nl/Kg_{cat}/h$. Feed composition: $CO = 1\%$ v/v, $O_2/CO = 0.4$, N_2 to balance; atmospheric pressure. Experimental (symbols) and calculated (solid lines) fractions are reported.

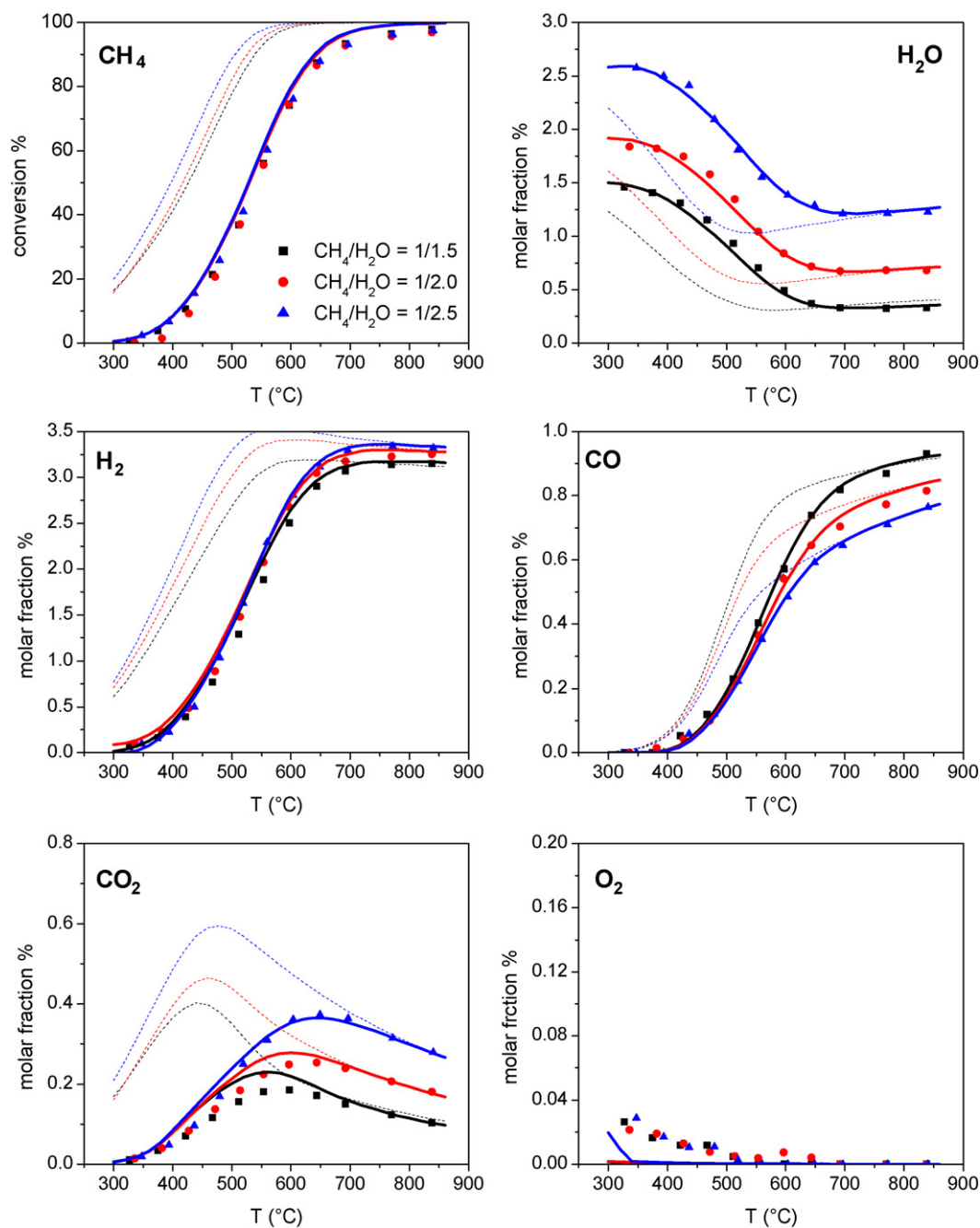


Fig. 10. Effect of H₂O addition on CH₄ conversion and products molar fractions in CH₄ steam reforming. Experimental (symbols) and calculated (solid lines) fractions are reported. Feed composition: (■) CH₄/H₂/O₂ = 1/1.5/0.75 v/v; (●) CH₄/H₂/O₂ = 1/2.0/1.0 v/v; (▲) CH₄/H₂/O₂ = 1/2.5/1.25 v/v; N₂ to balance; GHSV = 2 × 10⁶ Nl/K_{cat}/h; atmospheric pressure.

from the reverse water gas shift experiments, k_{H_2} and k_{CO} from the rich-combustion experiments. Optimal estimates were then obtained by regression over the entire data, including, at this stage, all the CPO tests. In the regression procedure, the model responses (the outlet molar fractions of methane, CO, CO₂, H₂ and H₂O) were weighted so that priority was given to best fit the CPO tests (and especially those on the effects of feed composition), while the agreement with the single sets of data was relaxed.

4.1. Kinetic analysis

Model predictions are reported in Figs. 2, 4–7, 9–11 as solid lines.

4.1.1. CH₄ total oxidation

All the CPO tests that were characterized by non-complete conversion of O₂ were treated as CH₄ oxidation data. The experiments at varying O₂/CH₄ ratio (Fig. 6) clearly indicated that the rate of CH₄ combustion is independent of O₂ con-

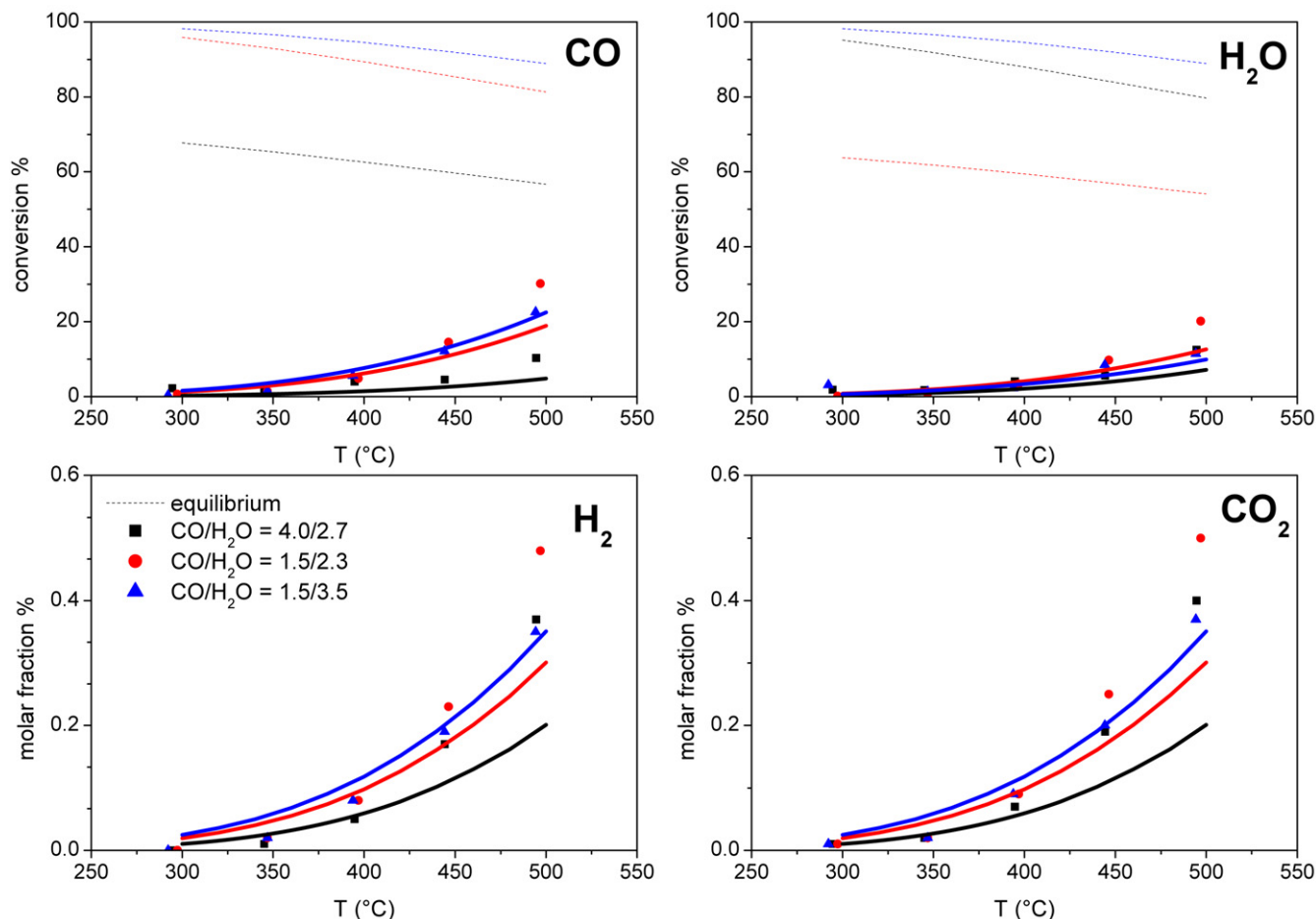


Fig. 11. Effect of reactants concentration on CO and H₂O conversion and products molar fractions in the WGS. Experimental (symbols) and calculated (solid lines) fractions are reported. Feed composition: (■) CO/H₂O = 4.0/2.7 v/v; (●) CO/H₂O = 1.5/2.3 v/v; (▲) CO/H₂O = 1.5/3.5 v/v; N₂ to balance; GHSV = 2×10^6 Nl/K_{gcat}/h; atmospheric pressure.

centration, since no effect was detected in the low temperature range ($T < 450$ °C) upon increasing the O₂ inlet fraction. The H₂O co-feed tests (Fig. 4) showed a moderate inhibition of CH₄ combustion: this effect was little influenced by the varying amount of H₂O, suggesting that the available surface sites for H₂O adsorption were close to saturation. On the opposite, CO₂ injection (Fig. 5) did not affect the reaction process in the whole temperature range. When the concentration of the reactants was increased (Fig. 7), a strong decrease of CH₄ and O₂ conversion was observed. On the basis of these observations, the following expression is proposed:

$$r_{\text{totox}} = \frac{k_{\text{totox}} P_{\text{CH}_4}}{1 + k_{\text{adH}_2\text{O}} P_{\text{H}_2\text{O}}} \sigma_{\text{O}_2}. \quad (1)$$

The term σ_{O_2} is defined as follows:

$$\sigma_i = \frac{P_i}{P_i + 10^{-6}}, \quad i = \text{O}_2. \quad (2)$$

Given the independence of the rate of CH₄ total oxidation from O₂, such term is necessary for correctly describing the situation of absence of the co-reactant (that is $r_{\text{OX}} = 0$ at $P_{\text{O}_2} = 0$). The choice of a tolerance value of 10^{-6} atm has no specific physical meaning. It is the minimum value which guarantees numerical convergence in the simulations. Sensitivity analysis reveals

negligible variations in the calculated results for values up to 10^{-4} atm.

The absence of any dependence on the O₂ content in the reaction rate is coherent with the picture of a catalytic surface almost completely covered by O* adatoms, with a few sites for CH₄ adsorption, as pointed out in the literature by experimental results over Rh [36] and by numerical simulations with detailed kinetic models [14,29].

The estimated activation energy for methane oxidation amounts to 92 kJ/mol. This value is in satisfactory agreement with the estimate by Deshmukh and Vlachos [37] of an apparent activation energy for methane oxidation over Rh of 100 kJ/mol (based on a reduced microkinetic model) and experimental estimates of 84 kJ/mol [38] and 113 kJ/mol [39], discussed by the same authors. Indeed, the activation energies of the successive CH_X-H bond breaking steps (involved in CH₄ activation over Rh) range between about 10 and about 30 kcal/mol, according to theoretical calculations [14,29].

4.1.2. CH₄ steam reforming

Steam reforming experiments at increasing H₂O content (Fig. 10) clearly indicated that CH₄ conversion is independent of H₂O inlet concentration within the investigated range. It is

Table 2
Kinetic scheme and parameter estimates

Reaction	Rate equation r_i [$\frac{\text{mol}}{\text{gcat s}}$]	$k_i^{873\text{K}}$ [$\frac{\text{mol}}{\text{atm gcat s}}$]	E_{act} [$\frac{\text{kJ}}{\text{mol}}$]
CH ₄ total oxidation CH ₄ + 2O ₂ → CO ₂ + H ₂ O	$r_{\text{tot ox}} = \frac{k_{\text{tot ox}} P_{\text{CH}_4}}{1 + k_{\text{ads H}_2\text{O}} P_{\text{H}_2\text{O}}} \sigma_{\text{O}_2}$	1.030×10^{-1}	92
CH ₄ steam reforming CH ₄ + H ₂ O ↔ 3H ₂ + CO	$r_{\text{SR}} = \frac{k_{\text{SR}} P_{\text{CH}_4} (1 - \eta_{\text{SR}})}{1 + k_{\text{ads CO}} P_{\text{CO}} + k_{\text{ads O}_2} P_{\text{O}_2}} \sigma_{\text{H}_2\text{O}}$	1.027×10^{-1}	92
Direct water gas shift CO + H ₂ O → CO ₂ + H ₂	$r_{\text{WGS}} = \frac{k_{\text{WGS}} P_{\text{H}_2\text{O}} (1 - \eta_{\text{WGS}})}{1 + k_{\text{ads H}_2\text{O}} P_{\text{H}_2\text{O}}} \sigma_{\text{CO}}$ $\eta_{\text{WGS}} < 1$	6.239×10^{-2}	25
Reverse water gas shift H ₂ O + CO → CO ₂ + H ₂	$r_{\text{RWGS}} = k_{\text{RWGS}} P_{\text{CO}_2} (1 - \eta_{\text{RWGS}}) \sigma_{\text{H}_2}$ $\eta_{\text{WGS}} < 1$	1.276×10^{-2}	62
H ₂ oxidation H ₂ + $\frac{1}{2}$ O ₂ → H ₂ O	$r_{\text{H}_2 \text{ ox}} = k_{\text{H}_2 \text{ ox}} P_{\text{H}_2} \sigma_{\text{O}_2}$	2.638×10^3	62
CO oxidation CO + $\frac{1}{2}$ O ₂ → CO ₂	$r_{\text{CO ox}} = k_{\text{CO ox}} P_{\text{CO}} \sigma_{\text{O}_2}$	1.938×10^1	76
Surface adsorption	$k_{\text{ads } i}^{873\text{K}}$ [atm ⁻¹]		ΔH_{ads} [$\frac{\text{kJ}}{\text{mol}}$]
O ₂	5.461		-73
H ₂ O	3.901×10^2		-16
CO	2.114×10^2		-37

believed that the adopted technique of *in situ* H₂O production did not bias the results, since H₂ combustion was active at much lower temperatures than methane steam reforming.

Also the results of the H₂O-rich CPO tests (Fig. 4) confirmed the independence of the rate of steam reforming on the amount of H₂O: upon increasing the inlet H₂O content, no effect was observed on the conversion of CH₄ at temperatures higher than 450 °C (where O₂ was completely consumed and steam reforming uniquely contributed to CH₄ consumption). Similar conclusions were also drawn in the past, after an experimental investigation on Rh catalysts at low Rh loading [12].

The following expression was adopted,

$$r_{\text{SR}} = \frac{k_{\text{SR}} P_{\text{CH}_4} (1 - \eta_{\text{SR}})}{1 + k_{\text{ads CO}} P_{\text{CO}} + k_{\text{ads O}_2} P_{\text{O}_2}} \sigma_{\text{H}_2\text{O}}, \quad (3)$$

wherein the thermodynamic limit is respected by the term $(1 - \eta_{\text{SR}})$, η_{SR} being the ratio of the experimental reaction quotient $K_{\text{P,SR}}$ and the thermodynamic equilibrium constant $K_{\text{EQ,SR}}$. The term $\sigma_{\text{H}_2\text{O}}$ is defined by Eq. (2) with $i = \text{H}_2\text{O}$. It is worth noting that the adopted first-order dependence on CH₄, the independence from H₂O, and the estimate of the activation energy are in agreement with the findings of Wei and Iglesia [40,41], who verified the independence of CH₄ activation on the nature and the amount of the co-reactant for noble metal supported catalysts and proposed a unifying mechanism for all methane activation reactions (including cracking), wherein the only kinetic relevant step is the breaking of the first C–H bond. Besides, in the present work, the estimate of the intrinsic kinetic constant of steam reforming is practically coincident with that of methane oxidation; this further supports the hypothesis that the rate determining step of both reactions is related to methane pyrolysis.

Differently from the results of Wei and Iglesia [40,41], who studied the behavior of highly diluted feed mixtures, Eq. (3) includes an inhibition term due to the competitive adsorption of CO and O₂. Indeed, the CPO tests at varying dilution clearly showed that the overall kinetic order of the process is lower than 1. This effect can be well described by assuming that the surface is hindered by the adsorption of reacting species. We included an inhibiting effect due to CO adsorption after reforming experiments with co-feed of CO, which provided a direct evidence of reversible poisoning; they belong to the series of experiments devoted to the comparison between the rates of steam and dry reforming and are reported in Part II of the present study. Additional competitive adsorptions cannot be excluded, based on the present data; further experimental and theoretical investigations are presently in progress [42]. Concerning the inhibiting effect of O₂ adsorption, an important delaying effect of O₂ on the activation of steam reforming had been directly observed in the past on catalysts at low Rh loading [32]; in the case of the present 4 wt% Rh catalyst, a similar effect was indirectly deduced from the CPO tests with concentrated mixtures, wherein the formation of syngas shifted to higher temperatures than in the case of diluted feed mixtures. The estimates of $k_{\text{ads O}_2}$ and $\Delta H_{\text{ads O}_2}$ (reported in Table 2) are such that the calculated inhibition by O₂ is very limited for diluted feed streams, while it becomes important in the case of concentrated feed streams.

4.1.3. Water gas shift

Indirect pieces of evidences on the importance of the WGS reaction within the CPO reaction scheme were provided by the CPO tests with co-feed of H₂O and the steam reforming tests. In the former case, the addition of water did not affect the con-

version of methane but increased the H₂/CO ratio; in the latter case, CO₂ was produced together with the syngas mixture. Water gas shift tests at varying concentration of the reactants were performed to define the main kinetic dependences of its rate equation. In Fig. 11, data lie far from the equilibrium at all the investigated temperatures. The reaction appeared in fact relatively slow under the examined conditions. H₂O conversion did not change significantly upon increasing either H₂O concentration or CO concentration, while CO conversion decreased at increasing CO inlet concentration.

The following rate equation was adopted and provided a satisfactory agreement with data:

$$r_{\text{WGS}} = \frac{k_{\text{WGS}} P_{\text{H}_2\text{O}} (1 - \eta_{\text{WGS}})}{1 + k_{\text{adsH}_2\text{O}} P_{\text{H}_2\text{O}}} \sigma_{\text{CO}} \quad (4)$$

The term $(1 - \eta_{\text{WGS}})$ and the term σ_{CO} respectively account for the thermodynamic consistency of the equation and for the activation of the reaction only in the presence of the co-reactant. An additional constraint is given in Table 2: since a different equation is used for RWGS, Eq. (4) is valid only when the term η_{WGS} is lower than the unity. Equation (4) well agrees with the studies of Bunluesin et al. [43], who found a zero-order dependence on CO and first-order dependence on H₂O for ceria- and alumina-supported Rh catalysts when performing diluted WGS tests (15 Torr H₂O, 20 Torr CO).

Kinetic expression and parameters were refined on the basis of the CPO data. In particular, differently from the results reported by Bunluesin et al. [43], Eq. (4) contains an inhibition term due to H₂O adsorption. This term was introduced on the basis of CPO tests under concentrated conditions. Fig. 8b reports the experimental K_P to K_{EQ} ratio estimated for the WGS reaction in the CPO runs at decreasing dilution. In fact, while in highly diluted experiments (with CH₄ concentration lower than 4%) WGS was equilibrated, at increasing concentration of the reactants, the reaction progressively deviated from the equilibrium and became kinetically controlled: in the run with CH₄ and air, WGS resulted under kinetic control in the whole temperature range. These data are highly informative and point out that the WGS reaction is an effective route in the reaction pathway but it progressively slows down at increasing concentration of the reactants. The inhibition term due to H₂O was explicitly added in Eq. (4) in order to describe the progressive divergence of the WGS from the equilibrium. Though the parameters have been weighted giving priority to the CPO tests, Eq. (4) fits well also the single WGS and steam reforming data.

4.1.4. Reverse water gas shift

Experimental evidence which justify the rate equation assumed for RWGS is given in Part II of the present work. On the basis of independent RWGS tests, a rate equation was developed and introduced in the kinetic scheme of CPO. Though the contribution of RWGS was negligible in the CPO runs, numerical analysis of CPO and steam reforming data pointed out that it is not possible to use one equation comprising both the direct and the reverse WGS steps. The direct and the reverse steps must be treated as two distinct reactions with different kinetic dependences and a coherent approach to the equilibrium.

For this reason, in the model when RWGS is active (i.e. when $\eta_{\text{RWGS}} < 1$) the WGS rate is forced to be nil and vice versa, when WGS is active the RWGS rate is set equal to zero.

The following rate equation was adopted:

$$r_{\text{RWGS}} = k_{\text{RWGS}} P_{\text{CO}_2} (1 - \eta_{\text{RWGS}}) \sigma_{\text{H}_2} \quad (5)$$

The term $(1 - \eta_{\text{RWGS}})$ and the term σ_{H_2} respectively account for the thermodynamic consistency of the equation and for the activation of the reaction in the presence of the co-reactant. Equation (5) reports that under the investigated conditions RWGS is first order dependent on CO₂ and independent of H₂. As for the WGS rate, Eq. (5) is the simplest one which best describes the data.

4.1.5. H₂ and CO oxidation

On 0.5 wt% catalysts [12], H₂/CO ratios lower than 2 had been observed in highly diluted CPO tests at low temperatures and very high GHSV values (up to 10.5×10^6 Nl/K g_{cat}/h) and could not be justified on the basis of the contributions of WGS and steam reforming alone; the inclusion of H₂ and CO post-combustions in the indirect kinetic scheme allowed to correctly describe those data, in particular the “H₂ deficiency” observed in the presence of unreacted O₂. In the present investigation, the 4% Rh catalyst was so active that, under diluted conditions, the measured H₂/CO ratios were always close to 2 even at varying GHSV. However, under concentrated conditions the overall process rate was moderated and deviations of the measured H₂/CO ratio from the equilibrium (Fig. 8a) were observed. With CH₄/air mixtures, the ratio was always below the equilibrium and reached of the value of 2 only at 850 °C. This effect could not be properly described, but by introducing independent reaction pathways for H₂ and CO, that is by accounting for H₂ and CO consecutive oxidations.

Independent fuel-rich tests were carried out for tuning of the corresponding kinetics.

Data showed that H₂ oxidation was active at much lower temperature than CO oxidation (100 °C vs 175–200 °C), and both reactions were much more active than CH₄ oxidation (typically active at 300–350 °C). The reactivity scale $r_{\text{OXH}_2} > r_{\text{OXCO}} \gg r_{\text{OXCH}_4}$ was evident.

The following simple expressions were adopted for the quantitative analysis:

$$r_{\text{OXH}_2} = k_{\text{OXH}_2} P_{\text{H}_2} \sigma_{\text{O}_2}, \quad (6)$$

$$r_{\text{OXCO}} = k_{\text{OXCO}} P_{\text{CO}} \sigma_{\text{O}_2}. \quad (7)$$

First-order rates were adopted, in line with the kinetics of CH₄ combustion. Accordingly, the limiting term σ_{O_2} was accounted for. The kinetic parameters in Eqs. (6) and (7) were initially estimated on the basis of the independent H₂ and CO rich combustion experiments and further refined in the general regression of the CPO data. Referring to Table 2, at 600 °C the estimated H₂:CO:CH₄ reactivity scale corresponds to 2000:200:1, much wider than that reported for low Rh content catalysts [12].

The final model predictions in Fig. 9 are characterized by important overestimations of the measured fuel conversion at the highest GHSV, where incomplete O₂ conversion was observed (which means that the extent of oxidation was out of

stoichiometric control). This lack of fit can be explained by assuming that the real mass transfer coefficient was lower than the theoretical value of a perfectly concentric annulus (included in the model). Indeed, the simulations recovered the experimental trends by adopting a value of the asymptotic Sh number of 4 (vs 5.8 for concentric annular duct). It is worth considering that a very limited extent of eccentricity can explain a significant decrease of the Sh number [34]. On purpose we did not treat the asymptotic Sh number as an adaptive parameter, since the estimate of the intrinsic kinetics was practically unaffected.

An underestimation of the real extent of mass transfer limitations could also explain the tendency of the model to predict smaller H₂ and CO concentrations than those observed at 450–500 °C. In the presence of a small degree of eccentricity of the annular duct, in fact, the O₂ concentration at the catalyst wall should decrease at increasing temperature more rapidly than predicted for a concentric annular duct, thus extinguishing the inhibiting effect on steam reforming and favoring syngas formation at lower temperatures (even with residual O₂).

4.2. Model adequacy

The adequacy of the reaction scheme and of the kinetic expressions was evaluated from the overall goodness of fit and from the physical consistency of the parameter estimates.

We also evaluated the function

$$S = \sum_{i=1}^{N_{\text{run}}} \frac{1}{s_i^2} \sum_{j=1}^{N_{\text{resp}}} (y_{ij} - y_{ij}^{\text{calc}})^2$$

with a total number of runs $N_{\text{run}} = 452$ and number of model responses $N_{\text{resp}} = 5$. S amounts to about $1\text{E}+03$. S exhibits a χ^2 distribution with $\nu = (N_{\text{run}} \times N_{\text{resp}} - 18 \text{ parameters})$ degrees of freedom if s_i^2 is replaced by σ_i^2 , the expected value of s_i^2 . Assuming that the available values of s_i^2 (evaluated from 5 replicates of standard CPO tests) were good estimates of σ_i^2 , than the realization of S should be compared with the value of $\chi_{\nu,0.95}^2$, which tends to ν , for large values of ν as in this case. Indeed $S < \nu$. However, it is recognized that the significance of such a test is questionable in the absence of robust estimates of the error variance for the various responses.

5. Concluding remarks

The present work reports an extensive kinetic investigation of the catalytic partial oxidation of CH₄ over a 4 wt% Rh/ α -Al₂O₃ catalyst. Activity tests under controlled conditions were performed in a wide experimental field (CH₄ = 1–27%, GHSV = 8×10^5 – 4.5×10^6 Nl/K g_{cat}/h, O₂/CH₄ = 0.56–1.3, H₂O- and CO₂-enriched feeds), exploiting the flexibility of the annular reactor. In the literature, a strong need exists for kinetic data of CH₄-CPO under representative conditions and, in this respect, the present experimental campaign constitutes a valuable set. On the basis of a 1D model of the annular reactor, a molecular kinetic scheme was developed, consisting of 6

reactions and 18 kinetic parameters. Rate expressions and kinetic parameters were tuned on the CPO tests, and to additional steam reforming, WGS, H₂ and CO oxidation tests. The resulting scheme accurately describes the reactants conversion and the products distribution and accounts for all the observed effects in a very large experimental field, which also comprises the side reactions. While efforts are being spent for developing a detailed kinetic scheme of the process and gaining some insight of the surface chemistry (identification of the rate determining steps, analysis of the most abundant surface intermediate), it is believed that, due to the simplicity of the rate equations and to the economy of parameters, the availability of a molecular scheme is valuable. Molecular schemes provide an immediate picture of the main reaction pathways of the process, and reproduce the prevailing kinetic dependences. Also, they represent practical tools for design purposes.

From numerical and experimental results, the following conclusions can then be drawn:

- (1) The kinetics of CH₄-CPO are well reproduced even neglecting the CO₂-reforming reaction. The present analysis suggests that the effects of the operating variables on reactant conversion and product distribution are suitably described under the assumption that CH₄ is consumed by total oxidation and steam reforming alone.
- (2) From numerical analysis of the data, total oxidation and steam reforming of CH₄ show a first-order dependence on CH₄ concentration and a zero-order dependence on the co-reactant concentration. Still, both reactions manifest overall kinetic orders lower than 1, so that the rate of methane conversion and syngas production with concentrated methane/air feeds is considerably lower than that measured with diluted feed streams. Apparently, CH₄ total oxidation is moderately inhibited by H₂O adsorption. Steam reforming is delayed in the presence of O₂ and is influenced by the competitive adsorption of the reacting species. The nature of inhibition is uncertain and is presently under investigation though the means of theoretical analysis; still, data can be well described by assuming that the surface is saturated by the adsorption of CO (or syngas).
- (3) WGS and RWGS have independent kinetics and the overall CPO reacting system is best described by assuming two different rate equations. The contribution of RWGS reveals negligible in the investigated CPO conditions. In contrast, in CPO tests at low concentration of reactants, WGS is fast and limited by the equilibrium. In the presence of concentrated mixtures, WGS becomes increasingly slower and kinetically controlled. Its rate equation is found to be first order dependent on H₂O, independent of CO and inhibited by H₂O.
- (4) Due to the high activity of 4 wt% Rh/ α -Al₂O₃ catalysts, the kinetic role of H₂ and CO post-combustion is negligible with diluted feed streams. In the case of concentrated feed mixtures, the consecutive oxidations of H₂ and CO contrast the equilibration of the WGS reaction and exert a control on the H₂/CO ratio.

Acknowledgment

This work was financially supported by MIUR-PRIN2005, Rome.

Appendix A. Notation

x_i^B	bulk molar fraction of specie i th
x_i^W	wall molar fraction of specie i th
D_i	molecular diffusivity ($\text{m}^2 \text{s}^{-1}$)
D_μ	microporous diffusivity ($\text{m}^2 \text{s}^{-1}$)
D_M	macroporous diffusivity ($\text{m}^2 \text{s}^{-1}$)
$D_{\text{eff},i}$	effective diffusivity ($\text{m}^2 \text{s}^{-1}$)
z	axial coordinate (m)
z^*	dimensionless axial coordinate $z^* = z/d_h$
F_i	molar flow of species i (mol s^{-1})
F_{TOT}^0	total inlet molar flow (mol s^{-1})
F_i^*	dimensionless molar flow of specie i th $F_i^* = F_i/F_{\text{TOT}}^0$
R^*	aspect ratio $R^* = R_{\text{int}}/R_{\text{ext}}$
d_h	hydraulic diameter (m)
$\text{Pe}_{m,i}$	Péclet number $\text{Pe}_{m,i} = \text{Re} \text{Sc}_i$
v	average gas velocity (m s^{-1})
Re	Reynolds number $\text{Re} = vd_h/\nu$
Sc_i	Schmidt number $\text{Sc}_i = \nu/D_i$
$K_{c,i}$	mass transfer coefficient (m s^{-1})
$\text{Sh}_{\text{loc},i}$	local Sherwood number of specie i th $\text{Sh}_{\text{loc},i} = K_{c,i}d_h/D_i$
$z_{\text{Sh},i}$	$z^*/\text{Pe}_{m,i}$
r_j	reaction rate (mol $\text{s}^{-1} \text{g}_{\text{cat}}^{-1}$)
P_i	partial pressure of the i th specie (atm)
C_{TOT}^S	total concentration (mol m^{-3})
$C_{\text{O}_2}^S$	O_2 concentration at the catalyst wall (mol m^{-3})
$C_{\text{CH}_4}^S$	CH_4 concentration at the catalyst wall (mol m^{-3})
$C_{\text{CH}_4}^{S,\text{eq}}$	CH_4 equilibrium concentration at the catalyst wall (mol m^{-3})
a_i	coefficient for the fifth-order polynomial function for the axial temperature (Eq. (7) in Table 1)
W_{CAT}	catalyst weight (g)
S	geometrical surface area of the catalyst (m^2)

Greek symbols

ν	cinematic viscosity ($\text{m}^{-2} \text{s}^{-1}$)
$\nu_{i,j}$	stoichiometric coefficient of the i th specie in the j th reaction
α_i	$W_{\text{CAT}}d_hS^{-1}C_{\text{tot}}^{-1}D^{-1}$
δ_L	thickness of the catalytic layer (m)
ϕ_i	generalized Thiele modulus of specie i th (–)
η_i^∞	effectiveness factor of specie i th at $\phi \rightarrow \infty$
η_i	effectiveness factor of the i th
ε_M	macropore void fraction (–)
ε_μ	micropore void fraction (–)
σ_i	limiting factor for i th specie $\sigma_i = P_i/(P_i + 10^{-6})$

References

- [1] D.A. Hickman, L.D. Schmidt, *J. Catal.* 138 (1992) 267.
- [2] D. Neumann, M. Kirchhoff, G. Vesper, *Catal. Today* 98 (2004) 565.
- [3] P. Aghalayam, Y.K. Park, D.G. Vlachos, *Catalysis* 15 (2000) 98.
- [4] A.P.E. York, T. Xiao, M.L.H. Green, *Top. Catal.* 22 (2003) 345.
- [5] P.D.F. Vernon, M.L.H. Green, A.K. Cheetham, A.T. Ashcroft, *Catal. Lett.* 6 (1990) 181.
- [6] D.A. Hickman, L.D. Schmidt, *Science* 259 (1993) 343.
- [7] D.A. Hickman, L.D. Schmidt, *AIChE J.* 39 (1993) 1164.
- [8] L. Basini, K. Aasberg-Petersen, A. Guarinoni, M. Ostberg, *Catal. Today* 64 (2001) 9.
- [9] E.P.J. Mallens, J.H.B.J. Hoebink, G.B. Marin, *J. Catal.* 167 (1997) 43.
- [10] H. Heitnes Hofstad, J.H.B.J. Hoebink, A. Holmen, G.B. Marin, *Catal. Today* 40 (1998) 157.
- [11] J.C. Slaa, R.J. Berger, G.B. Marin, *Catal. Lett.* 43 (1997) 63.
- [12] I. Tavazzi, A. Beretta, G. Groppi, P. Forzatti, *J. Catal.* 241 (2006) 1.
- [13] D. Wang, O. Dewaele, A.M. De Groot, G.F. Froment, *J. Catal.* 159 (1996) 418.
- [14] R. Schwiedernoch, S. Tischer, C. Correa, O. Deutschmann, *Chem. Eng. Sci.* 58 (2003) 633.
- [15] O.V. Buyevskaya, D. Wolf, M. Baerns, *Catal. Lett.* 29 (1994) 249.
- [16] Z. Tian, O. Dewaele, G.B. Marin, *Catal. Lett.* 57 (1999) 9.
- [17] K. Walter, O.V. Buyevskaya, D. Wolf, M. Baerns, *Catal. Lett.* 29 (1994) 261.
- [18] O.V. Buyevskaya, K. Walter, M. Baerns, *Catal. Lett.* 38 (1996) 81.
- [19] E. Ruckenstein, H.Y. Wang, *J. Catal.* 187 (1999) 151.
- [20] M. Maestri, A. Beretta, G. Groppi, E. Tronconi, P. Forzatti, *Catal. Today* 105 (2005) 709.
- [21] K.L. Hohn, L.D. Schmidt, *Appl. Catal. A Gen.* 211 (2001) 53.
- [22] D.A. Hickman, L.D. Schmidt, *J. Catal.* 138 (1992) 267.
- [23] R. Horn, K.A. Williams, N.J. Degenstein, L.D. Schmidt, *Catal. Lett.* 110 (2006) 169.
- [24] R. Horn, K.A. Williams, N.J. Degenstein, L.D. Schmidt, *Chem. Eng. Sci.* 62 (2007) 1298.
- [25] R. Horn, K.A. Williams, N.J. Degenstein, L.D. Schmidt, *J. Catal.* 242 (2006) 92.
- [26] J. Mantzaras, *Catal. Today* 117 (2006) 394.
- [27] J.D. Grundwaldt, A. Baiker, *Catal. Lett.* 99 (2005) 5.
- [28] J.D. Grundwaldt, S. Hanneman, C.G. Schroer, A. Baiker, *J. Phys. Chem. B* 110 (2006) 8674.
- [29] A.B. Mhadeshwar, D.G. Vlachos, *J. Phys. Chem. B* 109 (2005) 16819.
- [30] A. Beretta, P. Baiardi, D. Prina, P. Forzatti, *Chem. Eng. Sci.* 54 (1999) 765.
- [31] I. Tavazzi, M. Maestri, A. Beretta, G. Groppi, E. Tronconi, P. Forzatti, *AIChE J.* 52 (2006) 3234.
- [32] T. Bruno, A. Beretta, G. Groppi, M. Roderi, P. Forzatti, *Catal. Today* 99 (2005) 89.
- [33] W. Ibashi, G. Groppi, P. Forzatti, *Catal. Today* 83 (2003) 115.
- [34] R.K. Shaha, A.L. London, *Laminar Flow Forced Convection in Ducts*, Academic Press, New York, 1978.
- [35] R.C. Reid, J.M. Prausnitz, B.E. Poling, *The Properties of Gases & Liquids*, McGraw-Hill, New York, 1987.
- [36] M. Li, E. Iglesia, in: *Proceedings of the 5th World Congress on Oxidation Catalysis*, Sapporo, Japan, 2005, p. 74.
- [37] S.R. Deshmukh, D.G. Vlachos, *Combust. Flame* 149 (2007) 366.
- [38] R. Burch, P.K. Loader, N.A. Cruise, *Appl. Catal. A Gen.* 147 (1996) 375.
- [39] J.G. Firth, H.B. Holland, *Trans. Faraday Soc.* 65 (1969) 1891.
- [40] J. Wei, E. Iglesia, *J. Catal.* 225 (2004) 116.
- [41] J. Wei, E. Iglesia, *J. Catal.* 224 (2004) 370.
- [42] M. Maestri, A. Beretta, G. Groppi, E. Tronconi, D.G. Vlachos, in preparation.
- [43] T. Bunluesin, R.J. Gorte, G.W. Graham, *Appl. Catal. B Environ.* 15 (1998) 107.